Supplementary Information (SI) for Journal of Materials Chemistry A.

Supplementary Information

Passivating Defects and Optimizing Interfaces to Boost the Comprehensive Performance of Carbon-Cathode Hole-Transport-Layer-Free $CsPbI_2Br$ Solar Cells via Ionic Liquid

Wenxuan Li[‡], Xueyan Ma[‡], Hai Liu, Hongyan Cheng, Zhengjun Meng, Xiaoyang Liu, Guodong Wan, Zhe Gao, Yali Li[*], Yujun Fu, Deyan He and Junshuai Li[*]

LONGi Institute of Future Technology, and School of Materials & Energy, Lanzhou University, 222 South Tianshui Road, Lanzhou, Gansu 730000, China.

*Corresponding authors. E-mail: liyli@lzu.edu.cn (Y. Li), jshli@lzu.edu.cn (J. Li).

‡These authors contributed equally.

Experimental Section

Materials

The following materials were procured from Xi'an Yuri Solar Co., Ltd: PbI_2, $PbBr_2$, CsI, and SnO_2 (12% in H_2O colloidal dispersion). N, N-Dimethylformamide (DMF, 99.5%) and dimethyl sulfoxide (DMSO, 99.9%) were procured from Shanghai Aladdin Biochemical Technology Co., Ltd. 1-butyl-3-methylimidazolium methanesulfonate ([BMIM][MS]) and 1-butyl-3-methylimidazolium trifluoromethanesulfonate ([BMIM][OTF]) (98%) were procured from Bide Pharmatech Ltd. Conductive carbon paste (OPV-CP1) was purchased from Yingkou OPV Tech New Energy Co., Ltd. All materials were utilized without further purification.

Precursor Preparation

The $CsPbI_2Br$ (0.8 м) precursor solution was prepared by dissolving PbI_2, $PbBr_2$, and CsI together in a mixture of DMF and DMSO (4:1 v/v) and stirring at 90 °C for 3 h. The IL additive solutions were prepared by dissolving [BMIM][MS] and [BMIM][OTF] in DMSO, respectively.

Device Fabrication

The ITO glass substrates were subjected to a sequential ultrasonic cleaning process, wherein they were immersed in anhydrous ethanol, acetone and isopropanol each for 15 minutes. The ITO sides of the dried substrates were subjected to ultraviolet ozone treatment for 40 minutes. The 12 wt% aqueous dispersion of SnO_2 was first diluted to 3wt% with deionized water, then spin-coated on the pre-treated

ITO surface at 3000 rpm for 45 seconds and subsequently annealed at 150 °C for 30 minutes in ambient air. Subsequently, the resulting SnO_2-coated ITO glass was transferred to a N_2-filled glovebox. The $CsPbI_2Br$ precursor solution (with or without IL additive) was then spin-coated on the SnO_2-coated ITO glass at 3000 rpm for 60 seconds and subsequently annealed 160 °C for 10 minutes, thereby forming the pristine or acetate-added $CsPbI_2Br$ layer. Subsequently, the carbon electrode was fabricated by coating an 80 nm thick layer of conductive carbon paste onto the $CsPbI_2Br$ layer using a scraper and a shadow mask, followed by annealing at 100 °C for 1h in ambient air. Finally, conductive adhesive was affixed to both the carbon electrode and ITO, serving as the positive and negative electrodes respectively for the carbon-cathode HTL-free $CsPbI_2Br$ solar cell. The active area of the solar cell is 0.06 cm^2.

Density functional theory (DFT) calculation details

To analyze the electrostatic potential (ESP) and adsorption energy, the first-principal calculations were conducted utilizing spin-polarized density functional theory (DFT) within the Vienna ab initio simulation package (VASP 6.1) and the visualization of VESTA software. The electron exchange-correlation was described by the generalized gradient approximation of Perdew-Burke-Ernzerhof (GGA-PBE). The energy cutoff of the plane waves was set to 500 eV. A k-point grid of $3 \times 3 \times 1$ was selected for geometry optimizations. The force convergence criterion in geometric optimization was set to 0.01 eV/Å. For the electron self-consistent field calculations, the convergence criterion was set to 1×10^{-5} Ha. The (100) surface of

$CsPbI_2Br$ and (110) of SnO_2 with the lattice constants larger than 18 Å along the *z*-direction was adopted to avoid van der Waals force interactions. The isosurface value for the ESP is 0.02 eV $Å^{-3}$.

Characterization

The information regarding crystallization and material phases were determined by the multipurpose X-ray diffractometer (XRD, Malvern Panalytical Empyrean) with Cu K_α (λ = 1.5406 Å) radiation under 40 kV and 40 mA. The X-ray photoelectron spectroscopy spectra (XPS) and ultraviolet photoelectron spectroscopy (UPS) were recorded using an AXIS SUPRA + (Kratos Analytical) instrument, which is equipped with an Al K_α as the X-ray source (line width = 0.25 eV, maximum power = 600W). Fourier transform infrared spectroscopy (FTIR, Thermoscientific Nicolet iS50) was employed to analyze the interactions between functional groups. The morphologies were examined using field-emission scanning electron microscopy (SEM, Thermoscientific Apreo S), and the surface roughness was evaluated through an atomic force microscope (AFM, Cypher S-IDS) with a laser interference multi-physical field sensing imaging system. Water contact angles were obtained using an optical contact angle measuring apparatus (JGW-360B) with 5 μL droplets at room temperature. The absorbance properties were characterized by a UV-vis-NIR spectrophotometer (UV, Hitachi Ltd UH4150) within the 300-800 nm wavelength range. The steady-state photoluminescence (SSPL) spectra and time-resolved photoluminescence (TRPL) spectra were obtained on an FLS920 spectrofluorometer and a PicoQuant FluoQuant 300 with an excitation wavelength of 510 nm, respectively. The current density-voltage (*J*-*V*) characteristic curves, along with dark current-voltage (*I*-*V*) curves of the electron-only and hole-only devices, were measured using a Keithley 2400 source meter under standard solar irradiation (air mass (AM) 1.5G illumination, i.e., 100 mW cm^{-2}). The electrochemical impedance spectroscopy (EIS) measurements and the Mott-Schottky (MS) test were conducted on a CHI660E electrochemical workstation in the frequency range of 10^{-1} to 10^{6} Hz at an AC voltage with a 10 mV amplitude. The external quantum efficiency (EQE) spectra were measured using a solar cell external quantum efficiency testing system (Zolix, SCS600). The stability was evaluated in a glovebox under different temperatures.

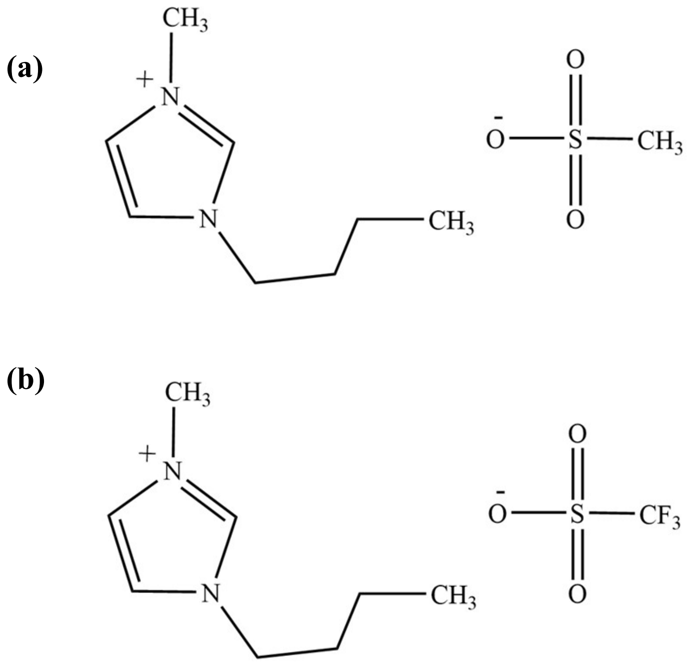

Figure S1. The chemical structure of (a) [BMIM][MS] and (b) [BMIM][OTF].

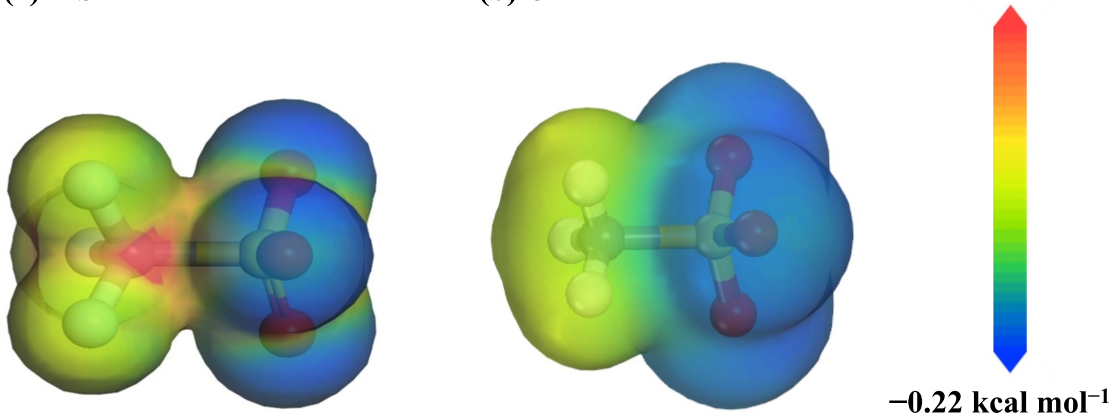

(a) MS$^-$ **(b)** OTF$^-$

(c) BMIM$^+$

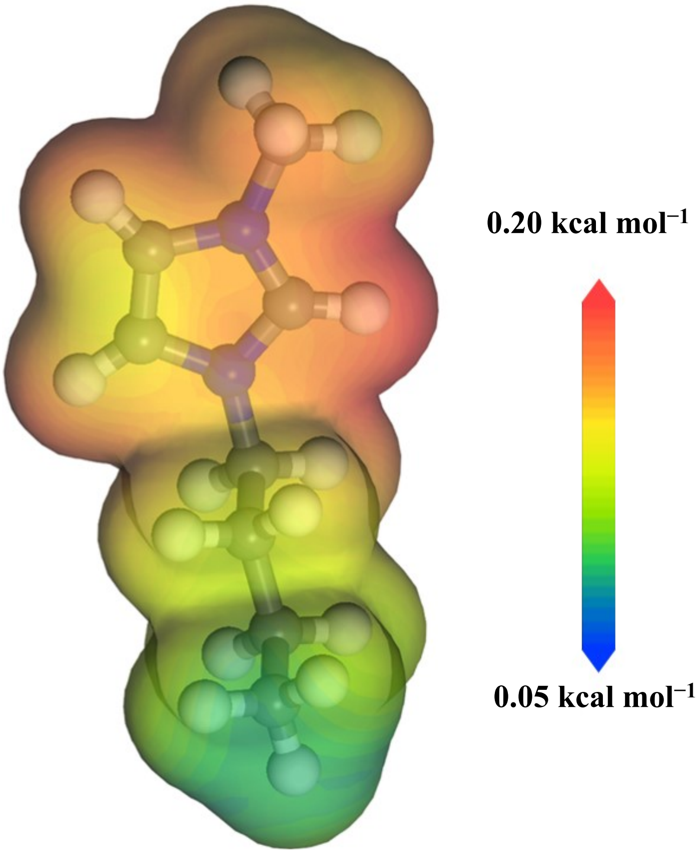

Figure S2. EPS of (a) MS$^-$, (b) OTF$^-$, and (c) BMIM$^+$.

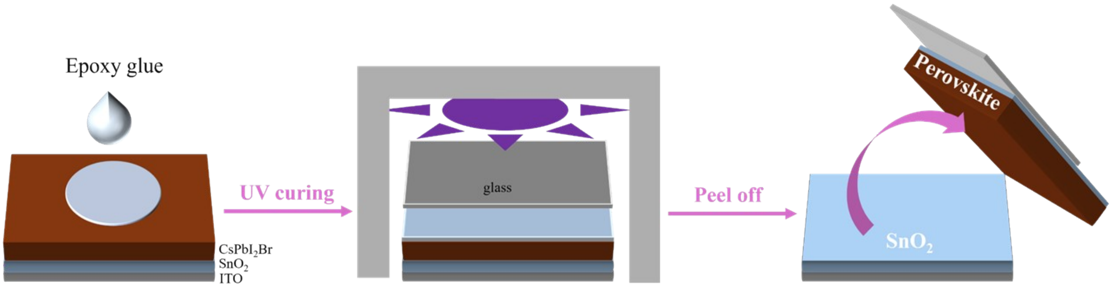

Figure S3. Schematic diagram of peeling off $CsPbI_2Br$ with the photosensitive adhesive.

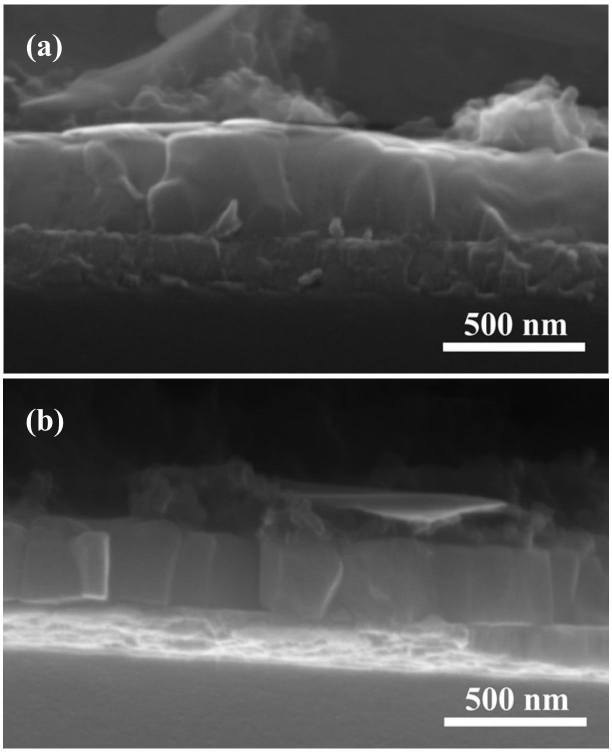

Figure S4. Cross-sectional SEM images of the (a) pristine and (b) [BMIM][OTF]-added $CsPbI_2Br$ layers on SnO_2.

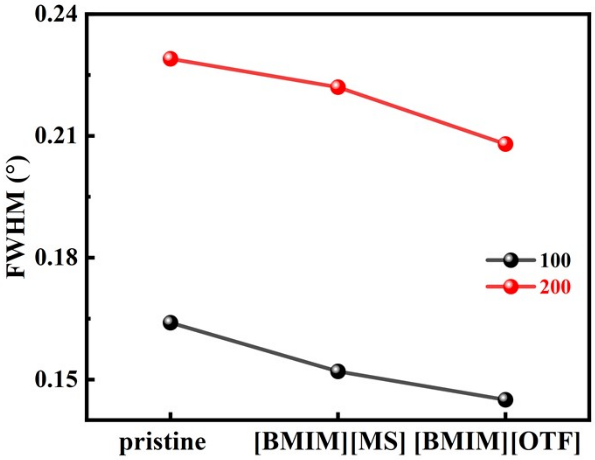

Figure S5. FWHM values of the (100) and (200) peaks of the pristine and IL-added $CsPbI_2Br$ films.

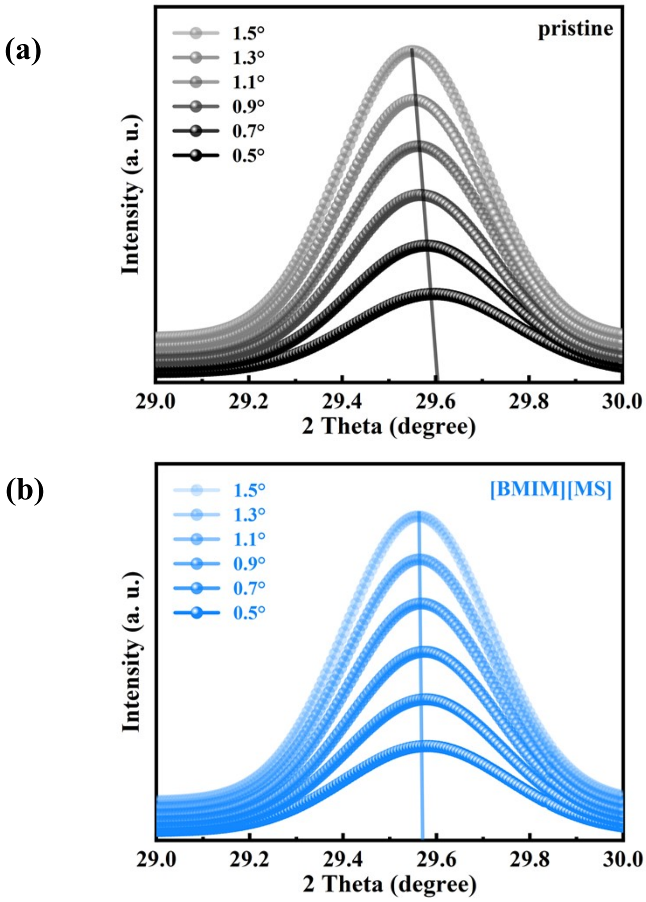

Figure S6. GIXRD spectra of the (a) pristine and (b) [BMIM][MS]-added $CsPbI_2Br$ films.

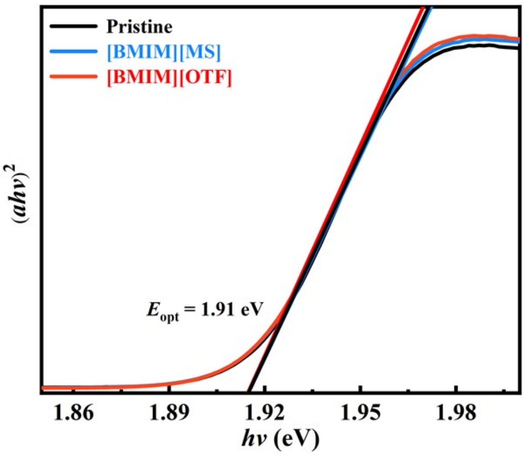

Figure S7. Tauc plots of the pristine and IL-added $CsPbI_2Br$ films.

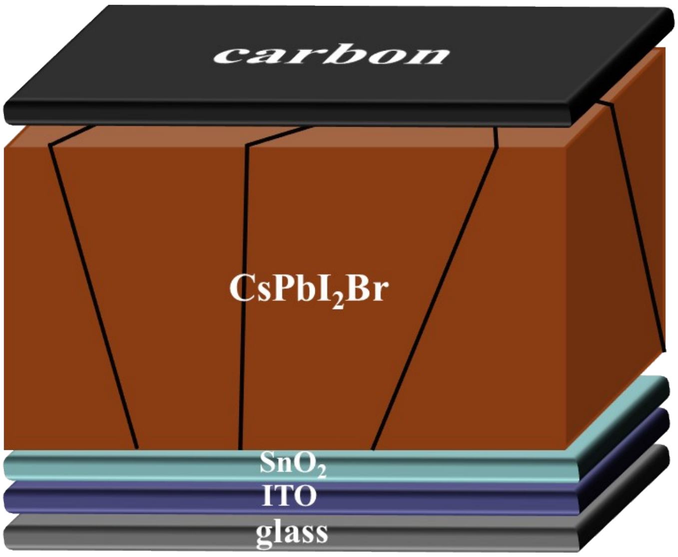

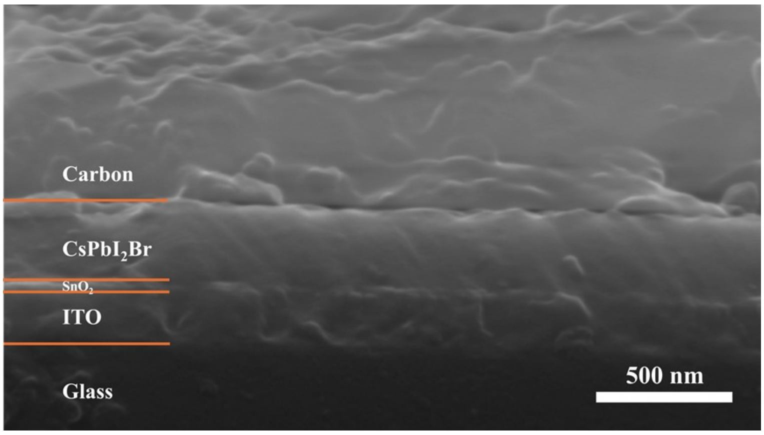

Figure S8. Device schematic and cross-sectional SEM image of a carbon-cathode HTL-free $CsPbI_2Br$ solar cell.

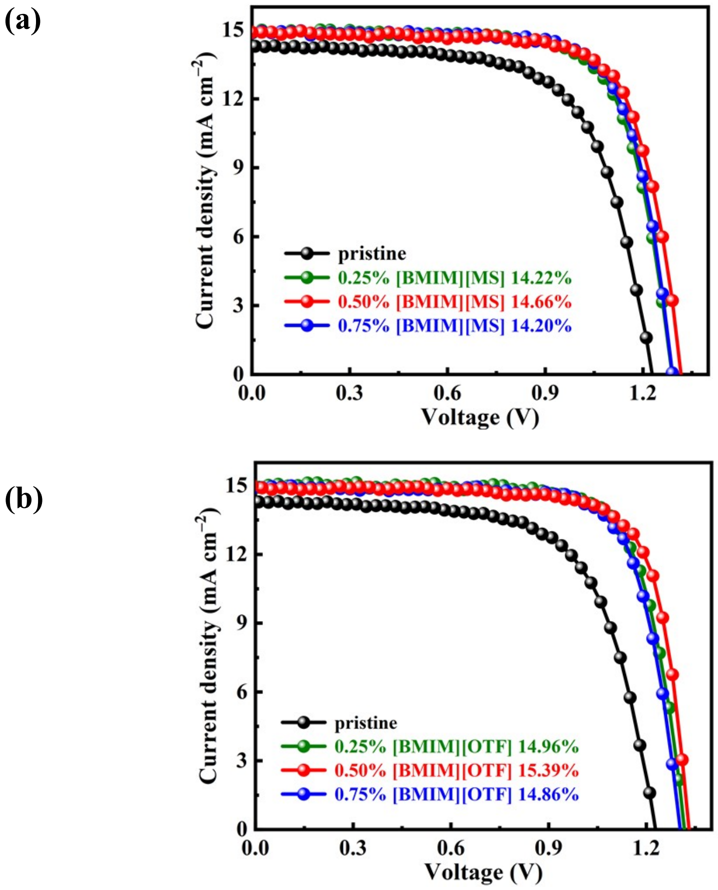

Figure S9. Illuminated *J*-*V* curves for the devices with various concentrations of (a) [BMIM][MS] and (b) [BMIM][OTF]. (0.25-0.75% represents the molar ratios of each additive to $CsPbI_2Br$, the same as below)

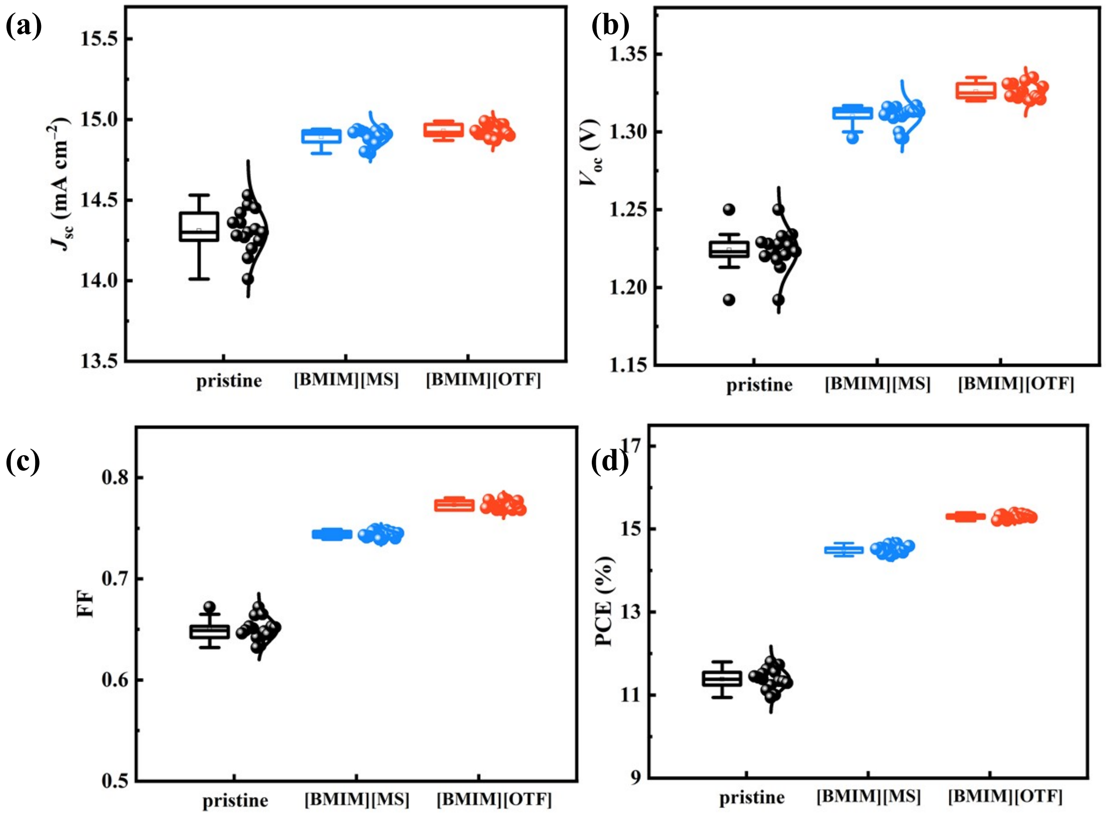

Figure S10. Statistical charts of (a) J_{sc}, (b) V_{oc}, (c) FF and (d) PCE of 15 independent devices at the optimal concentration of 0.50% for each batch.

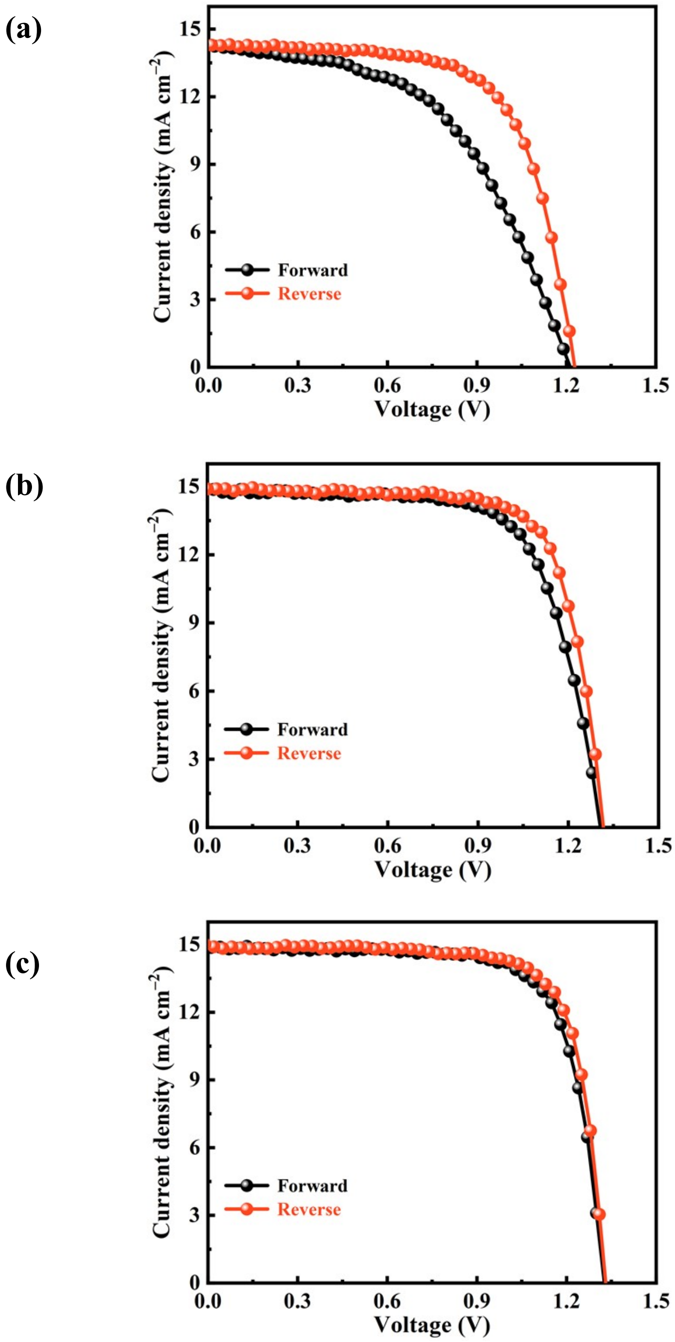

Figure S11. Illuminated *J*-*V* curves of the champion devices under the reverse scan (RS) and forward scan (FS): (a) the pristine device, (b) the [BMIM][MS]-added device and (c) the [BMIM][OTF]-added device.

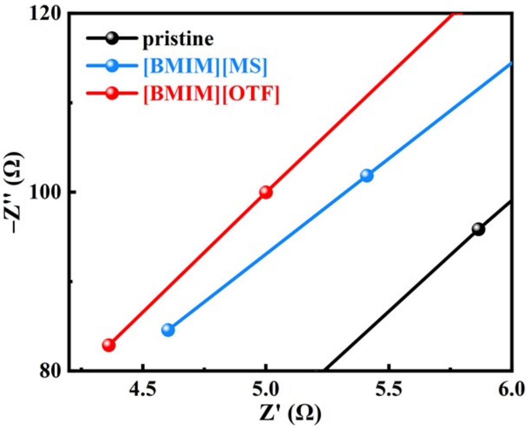

Figure S12. Enlarged plots of the EIS curves at high frequency for the pristine and IL-added devices.

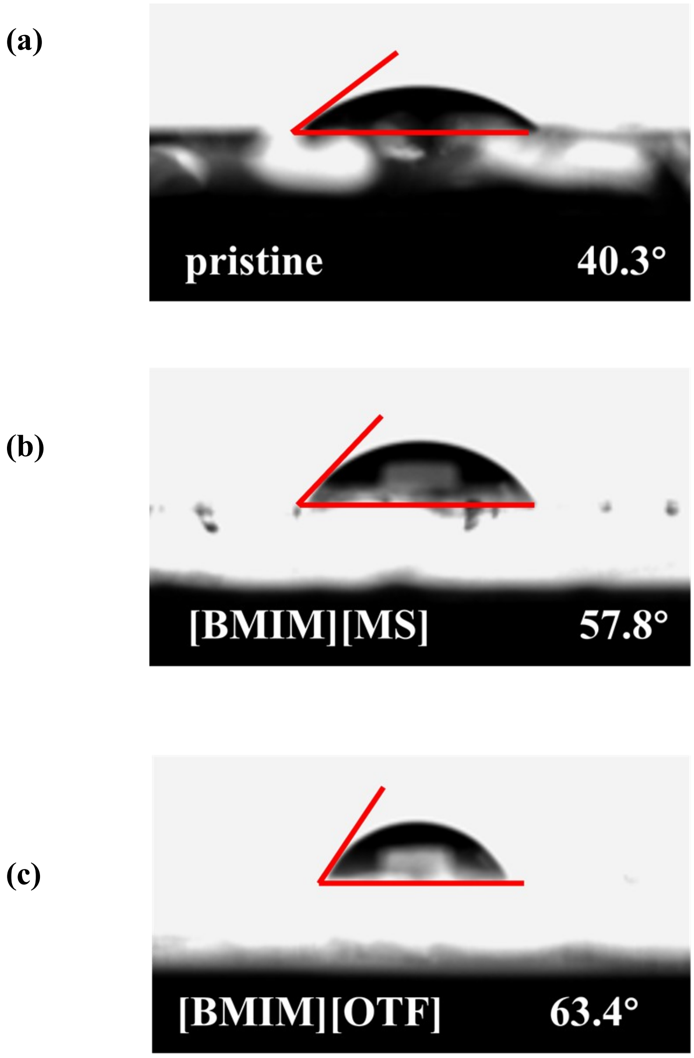

Figure S13. Water contact angles of the (a) pristine, (b) [BMIM][MS]-added and (c) [BMIM][OTF]-added $CsPbI_2Br$ films.

Table S1. Carrier lifetimes estimated from the TRPL spectra of Figure 4d.

Device	**τ_1 (ns)**	**τ_2 (ns)**	**A_1**	**A_2**	**τ_{ave} (ns)**
pristine	0.46	18.55	1628.59	188.15	16.01
[BMIM][MS]	0.13	8.61	1066.34	56.82	6.04
[BMIM][OTF]	0.12	6.84	869.01	51.07	4.28

Table S2. Carrier lifetimes estimated from the TRPL spectra of Figure 4h.

Device	τ_1 **(ns)**	τ_2 **(ns)**	A_1	A_2	τ_{ave} **(ns)**
pristine	1.19	42.87	1221.67	137.01	31.46
[BMIM][MS]	4.44	71.70	443.34	24.74	58.09
[BMIM][OTF]	4.63	96.76	312.57	13.74	96.31

Table S3. Summary of the reported photovoltaic parameters of the carbon-cathode HTL-free $CsPbI_2Br$ solar cells with PCEs over 15%.

Strategy	J_{sc} (mA cm^{-2})	V_{oc} (V)	FF (%)	PCE (%)	Ref
FTO/SnO_2/$CsPbI_2Br$ (cytosine)/C	14.72	1.317	77.34	15.00	25
FTO/TiO_2/$CsPbI_2Br$/Mxene+GO/C	14.90	1.290	78.25	15.04	26
FTO/c-TiO_2/$CsPbI_2Br$ (Tanshinone IIA)/C	14.71	1.328	77.40	15.12	13
ITO/SnO_2/$CsPbI_2Br$ (Tm(OTF)$_3$)/C	14.96	1.312	77.10	15.13	19
FTO/TiO_2/$CsPbI_2Br$ (MWCNTs)/C	14.85	1.291	79.00	15.14	14
FTO/TiO_2/$CsPbI_2Br$($CsPb_2I_4Br$)/C	14.60	1.32	79.1	15.25	15
FTO/TiO_2/$CsPbI_2Br$ (re-annealing in moist)/C	14.28	1.324	80.73	15.27	16
FTO/c-TiO_2/$CsPbI_2Br$(EMA)/C	14.40	1.344	79.43	15.37	21
FTO/TiO_2(MXene)/$CsPbI_2Br$/C	14.96	1.289	80.26	15.48	23
FTO/c-TiO_2/$CsPbI_2Br$(TRP)/carbon	14.76	1.300	80.85	15.51	22
ITO/SnO_2/$CsPbI_2Br$ (Y(Ac)$_3$)/C	14.90	1.338	77.90	15.53	28
FTO/c-TiO_2/$CsPbI_2Br$(cucurbituril)/C	14.69	1.305	81.14	15.59	20

Table S4. Summary of the photovoltaic parameters for the carbon-based HTL-free $CsPbI_2Br$ solar cells with or without IL additive.

Device		J_{sc} **(mA cm^{-2})**	V_{oc} **(V)**	**FF**	**PCE (%)**
pristine	Average	14.31 ± 0.30	1.224 ± 0.026	0.650 ± 0.020	11.38 ± 0.44
	Champion	14.30	1.228	0.672	11.80
[BMIM][MS]	Average	14.89 ± 0.05	1.310 ± 0.014	0.744 ± 0.005	14.51 ± 0.16
	Champion	14.90	1.316	0.747	14.66
[BMIM][OTF]	Average	14.93 ± 0.06	1.326 ± 0.009	0.773 ± 0.007	15.30 ± 0.10
	Champion	14.92	1.333	0.774	15.39

Note: We obtained the average values of these parameters from 15 independent devices of each batch.

Table S5. Photovoltaic parameters of the pristine and IL-added $CsPbI_2Br$ solar cells under FS and RS.

Device		J_{sc} (mA cm^{-2})	V_{oc} (V)	FF	PCE (%)	HI (%)
pristine	Reverse	14.30	1.228	0.672	11.80	23.4
	Forward	14.28	1.213	0.522	9.04	
[BMIM][MS]	Reverse	14.90	1.316	0.747	14.66	7.0
	Forward	14.86	1.306	0.702	13.63	
[BMIM][OTF]	Reverse	14.92	1.333	0.774	15.39	4.2
	Forward	14.85	1.326	0.749	14.75	

HI: hysteresis index.